# Examination of the solution to the hyperfine structure "puzzle" in H-like and Li-like $^{209}$Bi ions

F. F. Karpeshin
*Mendeleev All-Russian Research Institute of Metrology, 190005 Saint Petersburg, Russia*

M. B. Trzhaskovskaya
*Petersburg Nuclear Physics Institute of the National Research Center "Kurchatov Institute", 188300 Gatchina, Russia*

(Received 22 November 2017; revised manuscript received 4 June 2019; published 15 August 2019)

Some aspects of description of the Bohr-Weisskopf effect in hyperfine splitting (HFS) of the H- and Li-like ions of $^{209}$Bi are considered by application of the surface and volume models of the nuclear currents. Extension of these models, used in internal conversion theory, as a description of the HFS allows one to successfully describe the effect, without resorting to the specific difference. This is shown not to be needed at all. Moreover, it turns out to depend even more strongly on the nuclear model than the HFS values themselves. A comparison of the calculated HFS values to the experiment shows a satisfactory agreement. Both models provide an equally good description of the effect. However, they result in different values of the retrieved rms radius of the magnetization distribution over the nuclear volume. Prospects of future research are discussed.

DOI: 10.1103/PhysRevC.100.024326

## I. INTRODUCTION

Considerable progress during the past decades was achieved in the investigation of few-electron heavy ions at storage rings. Specifically, this concerns the study of their electronic structure and its influence on nuclear processes. On one hand, the possibility of accelerating the decay of nuclear isomers, or searching for the effect of the electron shell on alpha decay can serve as such examples (e.g., Ref. [1] and references cited therein). On the other, the understanding of atomic processes needs insight into the physics of the nuclei. Considerable attention has recently been paid to the study of the hyperfine structure of heavy ions, which is the subject of this paper. As compared to neutral atoms, a few-electron wave function can be calculated with high accuracy in heavy ions. However, QED effects give a significant contribution. This provides the basis to suggest that the hyperfine splitting (HFS) can be used to test QED (e.g., Ref. [2] and references cited therein). However, it was noted [2] that there is a stumbling stone on the way represented by the Bohr-Weisskopf effect [3]. The Bohr-Weisskopf effect is the correction to HFS caused by finite spatial distribution of magnetization over the nuclear volume as distinct from the interaction with a hypothetical point-like nucleus with the same magnetic moment. It has been known for decades that the Bohr-Weisskopf effect generates hyperfine magnetic anomalies in optical spectra of atoms. In the case of the $1s$ level in H-like ions of $^{209}$Bi, the contribution of the Bohr-Weisskopf effect to the HFS value constitutes approximately 2%. It slightly increases to 2.2% in the case of the $2s$ level in Li-like ions. On a higher level of accuracy, the Bohr-Weisskopf effect depends on the nuclear model. Some attempts were undertaken to calculate the Bohr-Weisskopf effect (Ref. [2] and references cited therein). They showed that there remains a contradiction with theory at the level of 20–30%. Such a result should be expected because nuclear calculations still cannot be performed *ab initio* in principle, in view of the absence of a small parameter [4]. At the same time, the Bohr-Weisskopf effect becomes essential for the description of experimental data, which gives rise to the statement of the bismuth hyperfine puzzle [5]. In view of this problem, another roundabout way was proposed in Ref. [2]. It runs that, instead of the calculation of the Bohr-Weisskopf effect, one can cancel its contribution in the specially constructed linear combination (difference) $\Delta' E$ [see Eq. (20) in Sec. III] of the HFS values of the H- and Li-like ions, being in the $1s$ and $2s$ states, respectively. The cancellation takes place if the parameter $\zeta$ in the combination [see Eq. (21) in Sec. III] is calculated in such a way that the Bohr-Weisskopf contribution is subtracted in the difference. This combination was called specific difference (SD). In the case of $^{209}$Bi ions, the calculated value of $\zeta = 0.16886$ was then listed to the fifth decimal [5–7].

We note, however, that, on the other hand, such a subtraction, aimed at mutual cancellation of small contributions from the Bohr-Weisskopf effect, also yields a considerable subtraction of the main terms. The errors add rather than subtract in the difference. This makes the result of subtraction, that is SD in our case, less accurate than the $1s$ and $2s$ HFS values themselves. We will see this in Sec. IV and Table I.

More specifically: For the method to work, it is necessary that parameter $\zeta$ be model independent. This idea seems to be incorrect, judging by the experience of the application of the theory of internal conversion (IC). It was subject to a critical check in Refs. [8,9]. At first sight, the application of IC theory may seem unusual for the HFS estimation. However, this idea is not new. For the first time, IC theory was applied in Ref. [10]. Then estimations of the HFS values and the related

 

TABLE I. HFS values $W_i$ for the $1s$ and $2s$ states (in eV), calculated with various representative model radii (in fm). The results are presented for the two values of the nuclear magnetic moment $\mu = 4.1106$ and 4.092 nuclear magnetons (see text). Each of the HFS values, listed in the table, may be equally well reproduced by either of the models: surface (SC) or volume (VC) magnetization currents, but with different model radii $R_c^{\rm SC}$ [Eq. (18)] and $R_c^{\rm VC}$[Eq. (19)], respectively. Note that the related rms radii of the models $R_2^{\rm SC}$ and $R_2^{\rm VC}$, respectively, turn out to be very similar, within 1%.

| $R_c^{\rm VC}$ | $R_2^{\rm VC}$ | $R_2^{\rm SC} \equiv R_c^{\rm SC}$ | $\mu = 4.1106$ | | $\mu = 4.092$ | |
|---|---|---|---|---|---|---|
| | | | $W_{1s}$ | $W_{2s}$ | $W_{1s}$ | $W_{2s}$ |
| 9.1214 | 7.4476 | 7.3703 | 5.06970 | 0.794952 | 5.04663 | 0.791378 |
| 8.6214 | 7.0393 | 6.9728 | 5.08041 | 0.796738 | 5.05729 | 0.793156 |
| 8.1214 | 6.6311 | 6.5745 | 5.09087 | 0.798484 | 5.06770 | 0.794894 |
| 7.6214 | 6.2228 | 6.1753 | 5.10106 | 0.800184 | 5.07784 | 0.796586 |
| 7.1214 | 5.8146 | 5.7754 | 5.11092 | 0.801830 | 5.08766 | 0.798224 |
| 6.6214 | 5.4063 | 5.3744 | 5.12042 | 0.803414 | 5.09711 | 0.799801 |
| 6.1214 | 4.9981 | 4.9726 | 5.12949 | 0.804927 | 5.10614 | 0.801308 |
| 5.6214 | 4.5898 | 4.5698 | 5.13809 | 0.806363 | 5.11470 | 0.802737 |

dynamic effect were performed in Refs. [11–13]. In the next section, we will show the relationship of these two phenomena in more detail. Meanwhile, based on the IC theory, the method of moments of the magnetization distribution was developed in Ref. [8] for the interpretation of the penetration effects. The method was applied in Ref. [9], where it was shown that the conclusion of the "hyperfine puzzle" was mostly due to underestimation of the model dependence of the SD. Indeed, it was anticipated in our paper [8] that such a puzzle could arise. Herein, we approach the problem in a different way as compared to that of Ref. [9]. We study the penetration effect on the HFS and SD values by means of comparison of the two conventional models, which are known to work well in the IC theory: surface (SC) [14] and volume (VC) [11,15] nuclear currents. In view of the fact that these models are, in some sense, opposite to each other in their characteristic features, one can say that the true result is somewhere in the middle.

In Sec. II, we briefly derive the formulas. In Sec. III, the relationship between IC and HFS is traced. The results of the calculations are reported in Sec. IV. Unexpectedly, we arrive at the conclusion that both of the models work equally well in the description of the data at the present level of precision. Although with different parameters the models result in the same values of the HFS for the $1s$ and $2s$ levels up to six decimals. However, the HFS values are quite sensitive to the only parameters of the models — their radii of the magnetization currents. The $\zeta$ and $\Delta' E$ values turn out to be more sensitive than the HFS values themselves, as expected. The results are discussed in more detail in the Conclusion.

When the paper was ready, Ref. [16] was issued. The authors showed that the value of the magnetic moment of the nucleus $\mu = 4.092$ nuclear magnetons may be more correct than 4.1106 [17] used previously. Such a value would essentially keep the present results, merely rescaling them by ~0.5%. For the sake of completeness, the rescaled values are also presented. They demonstrate the absence of any "hyperfine puzzle" within the present scope of the $^{209}$Bi issue: The data can be fairly explained with either of the magnetic moment values.

## II. DERIVATION OF THE FORMULAS

A Feynman graph of HFS is presented in Fig. 1. In the Furry's representation, the amplitude of the process can be expressed as

$$\mathcal{A}_F = \langle FM|H_c'|FM\rangle, \tag{1}$$

$$H_c' = \mathbf{j}_\mu(\mathbf{r})\mathbf{J}_\nu(\mathbf{R})D^{\mu\nu}(|\mathbf{r}-\mathbf{R}|), \tag{2}$$

where $\mathbf{j}_\mu(\mathbf{r})$, $\mathbf{J}_\nu(\mathbf{R})$ are the electronic and nuclear four-currents, respectively. We will designate $F, M$ the total angular momentum of the atom and its projection, as well as $I, M, j$ and $m$ — the nuclear spin and its projection, electronic angular momentum with its projection onto the quantization axis, respectively. Therefore, it is only the space three-component vector $\mathbf{J}_\nu(\mathbf{R})$ which gives a contribution. Equation (1) is expressed in terms of the atomic wave functions with a certain total angular momentum $F$ and its projection $M$:

$$|FM\rangle = \sum_m C(I\ M-m\ jm|FM)\ |I\ M-m\rangle|jm\rangle, \tag{3}$$

with $C(I\ M-m\ jm|FM)$ being the Clebsch-Gordan coefficients. By means of Eq. (3) one can go over from the $|FM\rangle$ to the $|IM\rangle|jm\rangle$ representation. The photon propagator

$$D^{\mu\nu}(R) = g^{\mu\nu}e^{i\omega|\mathbf{r}-\mathbf{R}|}/|\mathbf{r}-\mathbf{R}| = g^{\mu\nu}/|\mathbf{r}-\mathbf{R}| \tag{4}$$

reduces to the conventional Coulomb interaction for the transition energy $\omega = 0$. $g^{\mu\nu}$ in Eq. (4) is a metric tensor. Therefore, Eq. (1) can be written as

$$\mathcal{A}_F = \langle FM|\frac{\mathbf{j}(\mathbf{r})\mathbf{J}(\mathbf{R})}{|\mathbf{r}-\mathbf{R}|}|FM\rangle$$

$$= \langle FM|\mathbf{j}(\mathbf{r})\mathbf{J}(\mathbf{R})\sum_{LM}\frac{r_<^L}{r_>^{L+1}}Y^\star_{LM}(\hat{R})Y_{LM}(\hat{r})|FM\rangle. \tag{5}$$

In Eq. (5), $r_<$ ($r_>$) designates the smaller (larger) of the $r$ or $R$, and $\hat{r}$ stands for $\mathbf{r}/r$. Note that there is no need to put down the arguments of the spherical harmonics as $\hat{r}_<$ and $\hat{r}_>$: one always can put $\hat{r}_< = \hat{R}$ and $\hat{r}_> = \hat{r}$ with no loss of generality. The electronic current in the $|jm\rangle$ Eq. (3) reads

$$j_k(\mathbf{r}) = ie\bar{\psi}_{\kappa m_2}(\mathbf{r})\gamma_k\psi_{\kappa m_1}(\mathbf{r}), \tag{6}$$

with $\gamma_k$ the Dirac's matrices, and $\psi_{\kappa m_1}(\mathbf{r})$ the Dirac four-component electronic wave function. $\kappa$ is the relativistic quantum number, $\bar{\psi}_{\kappa m}(\mathbf{r}) = \psi^{+}_{\kappa m}(\mathbf{r})\gamma_0$.

The magnetic nuclear current generally can be expressed in a series over $\mathbf{T}^{(0)}_{LM}(\hat{R})$ — vector spherical harmonics. These are defined as follows [18,19]:

$$\mathbf{T}^{(\lambda)}_{LM} = \sum_{\nu} C(1\nu L + \lambda M - \nu | LM) Y_{L+\lambda M-\nu}(\hat{R})\xi_\nu, \quad (7)$$

with $\xi_\nu$ being three basic unit vectors, $L$ the multipole order of the transition, and $M$ the corresponding magnetic quantum number. Electrical nuclear currents can be expanded in a series over the spherical harmonics $\mathbf{T}^{(\pm 1)}_{LM}(\hat{R})$. But this is not our case: the Bohr-Weisskopf effect is related to the $M1$ interaction and $L = 1$, $\lambda = 0$ in Eq. (7). In the $|IM\rangle|jm\rangle$ representation, taking into account the Wigner-Eckart theorem, the coefficients of expansion $d_{LM}$ can be presented as follows [18,19]:

$$d_{LM} = \int \left(\mathbf{T}^{(0)}_{LM}(\hat{R}), \mathbf{J}(\mathbf{R})\right) d^2R = \frac{C(IM_1L0|IM_2)}{\sqrt{2I+1}} i J_L(R). \quad (8)$$

Integration in Eq. (8) is over the angular variables $d^2R$. Below we keep the name of the transition nuclear current for its radial component $J(R) \equiv J_1(R)$, omitting the multipole order $L = 1$.

Further derivation is straightforward. Passing to the $|IM\rangle|jm\rangle$ representation in Eq. (5) and making use of Eq. (8) allows one to integrate over the angular nuclear variable $\hat{R}$. Then integration over the electronic angular variable $\hat{r}$ can be performed by means of a formula [20]

$$\int \left(\mathbf{j}(\mathbf{r})\mathbf{T}^{(0)}_{1M}(\hat{R})\right) d^2r = \frac{C(jm_1 1M|jm_2)}{\sqrt{2j+1}} b, \quad (9)$$

with the reduced matrix element

$$b = i^{l-l'+1}\sqrt{\frac{3(2j+1)}{2\pi j(j+1)}}\kappa g(r) f(r), \quad (10)$$

where $g(r)$, $f(r)$ are the large and small components of the radial Dirac wave function. As a result, one arrives at the expression for the energy shift, containing a double integral over the radial variables of the nuclear and electronic currents

$$\mathcal{A}_F = 8e\pi\kappa(2j+1)\left[\frac{3(2l'+1)}{2j(I+1)}\right]^{1/2} R^{(2)}_\kappa, \quad (11)$$

$$R^{(2)}_\kappa = \int_0^\infty J(R) g(r) f(r) \frac{r_<}{r_>^2} R^2 dR\, r^2 dr. \quad (12)$$

The expression for the hyperfine splitting $W$ of the states with $F = I + j$ and $F = I - j$ follows Eq. (11):

$$W = (-1)^{(l-l'+1)/2}\frac{2e\kappa}{j+1}\sqrt{\frac{2\pi(2I+1)}{3I(I+1)}} R^{(2)}_\kappa. \quad (13)$$

In the first approximation, one can put in Eq. (13) $r_< = R$, $r_> = r$, neglecting the electron penetration effects into the nuclear range. In the IC theory, this approximation is known as the no penetration (NP) model. Then the double integral (12) factorizes into two separate integrals over the nuclear and electronic variables. By making use of the normalization

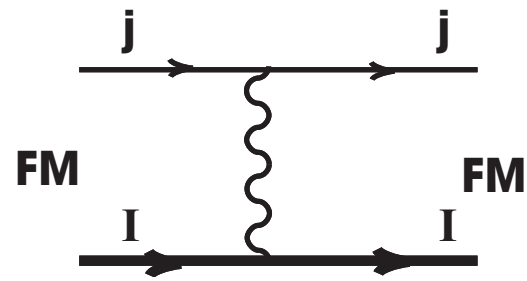


FIG. 1. Feynman graph of hyperfine shift. Nuclear propagator is shown by bold line. Atomic state is defined by the total momentum $F$ and its projection $M$, together with $I$ and $j$ — nuclear and electronic spins, respectively.

condition [3,8]

$$\int_0^\infty J(R) R^3 dR = \left[\frac{3(2I+1)(I+1)}{2\pi I}\right]^{1/2}\frac{e\hbar}{2M_p c}\mu, \quad (14)$$

the nuclear integral is reduced to the total magnetic moment of the nucleus $\mu$. The Bohr-Weisskopf effect is thus neglected in the NP approximation. For its description one has to take into account the electronic penetration effects. The SC and VC models describe well the penetration effects in IC. Their application is facilitated by the factorization of the double integral. Let us consider the extension of these models for the description of HFS's in more detail.

## III. RELATIONSHIP BETWEEN THE PHENOMENA OF INTERNAL CONVERSION AND HYPERFINE SPLITTING

The Feynman graph of IC is presented in Fig. 2. Actually, both graphs in Figs. 1 and 2 describe the same amplitude, though defined on different areas of the external kinematical variables of the transition energy and angular momenta. In quantum mechanics and theory of field, such values can be related to each other by making use of the analytical properties of the amplitudes, and the processes themselves are spoken about as crossing channels. The method of complex transition trajectories by Landau (e.g., Refs. [21,22]), or complex angular momenta by Regge [23] may set examples. In the

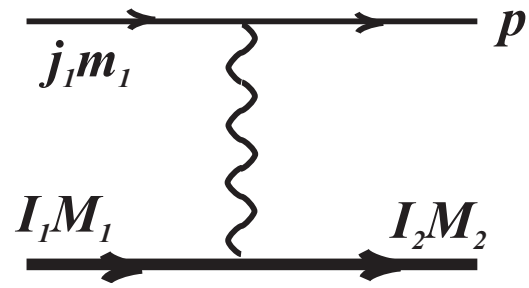


FIG. 2. Feynman graph of internal conversion. $I_1$, $M_1$, $I_2$, $M_2$ — nuclear quantum numbers (spins and their projections on the quantization axes) in the initial and final states, respectively. $j_1$, $m_1$ — electronic quantum numbers in the initial state. Conversion electron is characterized with the four-vector of its momentum $p$.

case of HFS, the analyticity of the amplitudes in Figs. 1 and 2 allows one to apply the methods, developed in the IC theory, to calculate the HFS values, considered as the diagonal IC matrix elements in the limit of the transition energy $\omega \to 0$.

The diagram in Fig. 2 hints that the amplitude of conversion transition factorizes into the amplitudes of virtual photon emission and its subsequent absorption by an atomic electron. There is exact factorization in the NP model, as well as in the SC and VC models. Internal conversion coefficients (ICC) are defined as the ratio of the probabilities of the conversion $\Gamma_c(\tau, L)$ and radiative $\Gamma_\gamma(\tau, L)$ transitions

$$\alpha(\tau, L) = \Gamma_c(\tau, L)/\Gamma_\gamma(\tau, L)\,, \tag{15}$$

where $\tau, L$ stand for the type and multipole order of the transition.

In the general case, calculations within the framework of various nuclear models need a two-dimensional integration over the electronic and nuclear variables within the nuclear volume (e.g., Ref. [8]). As a result, the factorization becomes approximate in the general case, as well as in $R_\kappa^{(2)}$, Eq. (12). This makes ICC $\alpha(\tau, L)$ model dependent, as well as HFS. In the IC theory, manifestations of the nuclear structure are classified into two kinds: static and dynamical effects (Refs. [14,24–29] and references cited therein). To the first kind belong the effects that arise because of change in the electronic wave functions as compared to the Dirac wave functions for the point-like nucleus. Coulomb wave functions are singular at the origin. Accounting for the finite charge distribution over the nuclear volume makes the functions regular, and brings about a correction to the ICC values up to 30% in the case of the $M1$ transitions in heavy nuclei [24,26]. Regarding Ref. [2], we note that it is directly pointed out therein that the authors realized the robustness of the $\zeta$ and $\Delta' E$ values as against variations of the parameters of Fermi charge distribution over the nuclear volume. This just comprises the static effect. Therefore, the conclusion of the model independence of SD [2] is only drawn from an investigation of the static effect, which is known not to be essential after the main shortcoming — the divergence of the Coulomb wave function — is, indeed, resolved.

The influence of a model for the transition nuclear currents on the ICC values is called the dynamical effect of the nuclear structure. This effect is responsible for the differences between the experimental ICC and their table values, which are observed in some cases of forbidden nuclear transitions. Note that these differences are also called anomalies in IC, similar to magnetic anomalies in the hyperfine spectra (e.g., Ref. [30]). The dynamical effect constitutes up to ∼10% in heavy nuclei in the case of the $M1$ transitions. The SC nuclear model was employed as the basis for a number of tables of ICC (e.g., Refs. [24,25]), in high demand for research and application purposes. The VC model is expected to work even better in the case of the valence $h_{9/2}$ proton orbital in $^{209}$Bi. Furthermore, the VC model was applied for the description of muonic conversion [11,15,31].

Turning now to HFS, we note that there are no transitions here. It is the distribution of the magnetization over the nuclear volume instead, which brings about the dynamical effect. To a certain extent, the dynamical effect on the HFS values in the Li-like ions was tested in Refs. [32,33], using two very close to one another nuclear models (see below). But not on the SD's, which was a concept that was proposed later. Actually, it was only in Ref. [8] that the SD values, calculated in different nuclear models, were compared to one another for the first time. There was a difference of 3% for the SD value, obtained by the authors of Ref. [8], which was a crucial divergence with the prediction of Refs. [2,6].

Assuming in Eq. (12) either surface $\delta$-like magnetization current $J(R)$, or a constant one within the nuclear volume, one arrives at the following expressions for HFS, allowing for the Bohr-Weisskopf effect:

$$\begin{aligned} W &= Nw, \\ w &= \int_0^\infty g(r)f(r)dr + t^\nu \equiv w_0 + t^\nu, \\ N &= -\frac{2(2I+1)}{I(j+1)} e\kappa\mu \frac{e\hbar}{2M_p c}. \end{aligned} \tag{16}$$

Here $j$, $I$ are the electronic and nuclear spins, respectively, $e$ is the elementary charge, $\mu$ the magnetic moment of the nucleus, and $\frac{e\hbar}{2M_p c}$ the nuclear magneton. $w_0$ gives the NP value. $t^\nu$, which we shall call the penetration matrix element, bears information on the nuclear structure

$$t^\nu = \int_0^{R_c} g(r)f(r)Y^\nu(r)\, r^2 dr, \tag{17}$$

with

$$Y^\nu(r) = \begin{cases} \frac{r}{R_c^3} - \frac{1}{r^2} & \text{for } \nu = \text{SC}, \quad (18) \\ \frac{1}{R_c^3}\left(4r - 3\frac{r^2}{R_c}\right) - \frac{1}{r^2} & \text{for } \nu = \text{VC} \quad (19) \end{cases}$$

In the NP model $Y^\nu(r) \equiv 0$. $R_c$ is the model radius of the transition currents. We refer upper index $\nu$ to the model, and lower index $i$ to the electronic level.

It is thus $t^\nu$ that only bears information about the Bohr-Weisskopf effect. It was proposed to get rid of it in the linear combination, called the specific difference [2,6]:

$$\Delta' E = W_{2s} - \zeta W_{1s}\,. \tag{20}$$

In terms of the penetration matrix elements (16), Eq. (20) has an evident solution

$$\zeta = t^\nu_{2s}/t^\nu_{1s}\,. \tag{21}$$

By making use of the last equation, SD (20) can be also expressed in equivalent form as follows:

$$\Delta' E = N\left(w_0^{2s} - \zeta w_0^{1s}\right) \tag{22}$$

$$= N w^{2s} \frac{p_{1s} - p_{2s}}{p_{1s}}\,, \tag{23}$$

where $p_i^\nu = t_i^\nu / w_i^\nu$ is the relative contribution of the Bohr-Weisskopf effect to the HFS. In view of that $p_{2s} > p_{1s}$, it follows from Eq. (23) that $\Delta' E < 0$.

Note that Eq. (18) for the SC model was used in Refs. [32,33] under the name of "homogeneous distribution." In terms of Eq. (18), model [32,33] is obtained by the

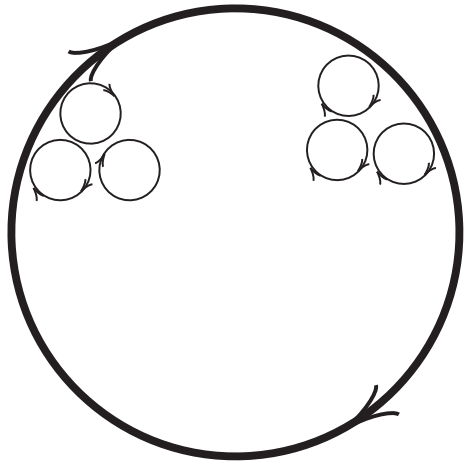

FIG. 3. Schematic picture explaining seeming contradiction of the terms of "homogeneous" and "surface-current" for the same nuclear model. Homogeneously distributed inside the nucleus magnetic dipoles are shown by elementary circular currents. In the bulk, the adjacent currents mutually cancel one another. As a result, only the encircling effective current survives, resulting in the surface-current model. It is this surface current which is responsible for the Bohr—Weisskopf effect.

replacement of $Y(r)$ with

$$\tilde{Y}^n(r) = \frac{r^{n+1}}{{R_c}^{n+3}} - \frac{1}{r^2}\,, \tag{24}$$

with the parameter $n = 0$ and 2. In a particular case of $n = 0$, Eq. (24) coincides with Eq. (18) in the case of the SC model. This seeming paradox of the names has a simple explanation on the physical ground. In fact, it is not the transition density, but rather the transition current that determines the HFS [see Eq. (2)]. On the other hand, such a classical picture of the "homogeneous" density distribution of elementary point-like magnetic dipoles gives rise to the effective current along the circle surrounding the locus, as inside the locus all the elementary currents mutually cancel one another. This directly generates the $\delta$-form nuclear current, as illustrated in Fig. 3. It is worth noting that another such paradox was found in Ref. [31]. It was found that muonic conversion from the collective nuclear states of giant dipole resonance is better described by the VC than the SC nuclear model, in spite of that, the transition nuclear density has a sharp maximum on the nuclear surface.

It is also worth noting some relations concerning the physical sense of the model parameters. In the VC model, $R_c$, like the equivalent electromagnetic radius, equals the radius of the sphere with the homogeneous sharp edge distribution of the magnetization currents. It is related to the rms radius $R_2$ by means of the following expression:

$$R_2^{\rm VC} = \sqrt{\frac{2}{3}} R_c^{\rm VC}\,. \tag{25}$$

In the SC model, all the multipole moments equal $R_i^{\rm SC} \equiv R_c^{\rm SC}$.

## IV. RESULTS OF CALCULATIONS

As was pointed out in the original paper by Bohr and Weisskopf, the effects of the nuclear structure can be studied by using a series expansion of the electronic wave functions within the nucleus [3]. Independently, the same series was also used in studies of the penetration effects in the cases of anomalous conversion [14,26]. In this way, the series expansion over the moments $R_2, R_4, \ldots$, of the nuclear magnetization distribution was developed for HFS in Ref. [8]. The leading term is proportional to the square of the rms radius ${R_2}^2$, or the second moment of the distribution of magnetization. Therefore, if two nuclear models have the same $R_2$, they will result in the same HFS in this approximation. This justifies the common procedure of studies of variations of $R_2$ by means of the hyperfine anomalies along isotopic chains (e.g., Refs. [34,35]).

Herein we systematize the result in such a way, which keeps minimum the difference between the results, obtained in the different models. For this purpose, we will fit the SC radius to the value that results in the same values of $w_{1s}$ and $w_{2s}$, as far as possible, to those obtained in the VC model, respectively. For this purpose, we note that both models only differ by the penetration matrix elements $t_i^{\nu}$. Given an $R_c^{\rm VC}$ radius, the fit of the $R_c^{\rm SC}$ radius was fulfilled by minimization of the following form:

$$\chi = \left|\frac{t_{1s}^{\rm SC} - t_{1s}^{\rm VC}}{t_{1s}^{\rm VC}}\right| + \left|\frac{t_{2s}^{\rm SC} - t_{2s}^{\rm VC}}{t_{2s}^{\rm VC}}\right|. \tag{26}$$

Even in such different models as the ones we use, the coincidence of the HFS values is achieved up to six decimals. For the purpose of better comparison to the experiment, we added the latest values of QED corrections to the calculated HFS values [6]: $\Delta E_{\rm QED}^{1s} = -0.0268$ eV, $\Delta E_{\rm QED}^{2s} = -0.005$ eV, and employed the contribution from the electron-electron interactions for the Li-like configuration from Ref. [6], where they were calculated up to the third order of $1/Z$: $\Delta E_{e-e}^{2s} = -0.030$ eV. The results are presented in Table I for various representative values of the radii of the models. In the first and third columns, $R_c^{\rm VC}$ and related $R_c^{\rm SC}$ radii are listed, respectively. The resulting rms radii turn out to be different in both models. To show this, we list the rms $R_2^{\rm VC}$ in the second column. In the SC model, $R_2^{\rm SC} \equiv R_c^{\rm SC}$. For the sake of clarity, the values obtained with $\mu = 4.092$, are also presented in columns 6 and 7. In both cases, either with $\mu = 4.1106$, or $\mu = 4.092$, the results can be adequately fitted to the last experimental values [16] of $W_{1s}^{\rm exp}$ = 5.08503(11) eV, and $W_{2s}^{\rm exp}$ = 0.797645(18) eV, although with different rms radii (also see below for more detail). The difference in radii compensates the variation of the magnetic moment of the nucleus.

Proceeding the discussion of the $\zeta$ and $\Delta' E$ properties, one can see from Eq. (26) that the condition of model independence of the $\zeta$ value is equivalent to the condition that both of the $t^{\nu}$ values, and therefore both of the $W_{1s}$ and $W_{2s}$ HFS's, might be fitted simultaneously by different models. This condition is looser than the mere proportionality of the $1s$ and $2s$ wave functions [2], not to mention that the proportionality is affected by the $e$–$e$ interactions in the case of Li-like configuration, QED effects, and so on. Naturally, if the

TABLE II. Parameters $\zeta$ and the SD values $\Delta'E$ (20), calculated in the VC and SC models, for the same representative values of the model radii as in Table I (for the sake of brevity, only the first column with the $R_c^{\rm VC}$ radius is kept). The SD values are presented in meV. As opposite to the $W_i$ values in Table I, model dependence of the $\zeta$ and SD values can be noted.

| $R_c^{\rm VC}$ | $\zeta^{\rm VC}$ | $\zeta^{\rm SC}$ | $\Delta'E$, VC | $\Delta'E$, SC |
|---|---|---|---|---|
| 9.1214 | 0.16688 | 0.16688 | −61.11 | −61.12 |
| 8.6214 | 0.16688 | 0.16689 | −61.12 | −61.14 |
| 8.1214 | 0.16689 | 0.16689 | −61.14 | −61.15 |
| 7.6214 | 0.16689 | 0.16689 | −61.16 | −61.17 |
| 7.1214 | 0.16689 | 0.16690 | −61.18 | −61.19 |
| 6.6214 | 0.16690 | 0.16690 | −61.20 | −61.21 |
| 6.1214 | 0.16690 | 0.16690 | −61.22 | −61.24 |
| 5.6214 | 0.16691 | 0.16691 | −61.25 | −61.26 |

equivalence of the models were complete, the $\zeta$ value would coincide in both models. Minor differences in the calculated $W_i$ values (of the order of $10^{-6}$ and less, beyond the accuracy of the numbers given in Table I), repeatedly increase, resulting in much greater differences in the $\zeta$ and $\Delta'E$ values, as illustrated in Table II for the same representative model radii as in Table I. In accordance with what was said previously, the difference of the $\zeta$ and $\Delta'E$ values as calculated in various models turns out to be much more than the difference of the HFS values themselves.

In the same rows, the $\zeta$ values hold up to five decimals, and $\Delta'E$ values only up to four decimals. The latter uncertainty is about the same as the experimental uncertainty [16] (which does not include the dynamical effect). Throughout Table II, the $\zeta$ values only coincide up to the fourth decimal, varying around 0.1669. And the $\Delta'E$ values differ already in the third decimal, varying between −61.3 and −61.1 meV. In both models, $\zeta$ and $\Delta'E$ values are sensitive to the only model parameter $R_c^{\nu}$.

In more detail, the results of the fit of the $W_i$ values within the framework of the VC model are presented in Table III, together with the experimental data. As one can see, the change in the $\mu$ value from 4.1106 to 4.092 is not crucial in the sense that a decrease in the nuclear magnetic moment can be compensated for by a decrease in the radius of magnetization currents without degrading the fit. Our present fit, reproduced in Table III, corresponds to the following values of the $R_2^{\rm VC}$ moment of the magnetization distribution: $R_2^{\rm VC} = 6.829$ fm in the case of $\mu = 4.1106$, and $R_2^{\rm VC} = 5.960$ fm in the case of $\mu = 4.092$. A similar fit can be performed using the SC model. The results obtained in Ref. [8] within the framework of the two-parameter magnetic moment method are also presented. They are in good agreement with the present calculations. For comparison, the results of Refs. [6,16] are also listed. One can see that the results of Ref. [6] are in worse agreement with the experiment. In contrast, the authors of Ref. [16] were quite satisfied by their fit. This is the key point to understanding the $^{209}$Bi hyperfine puzzle. As a matter of fact, the authors of Ref. [16] compare to the experiment, not the $W_i$ values themselves, but the SD values instead, which they designed for this purpose. No puzzle arises if the problem is approached in a more straightforward way, fitting the $W_i$ values.

## V. CONCLUSION

Usage of the hyperfine structure in few-electron ions for testing QED is a challenging task. The main uncertainty on this way looks to be the Bohr-Weisskopf effect. It makes a contribution at the level of 2% to the HFS of the 1$s$ and 2$s$ levels. At the same time, its correct *ab initio* calculation currently appears not to be a feasible task. The previous consideration is devoted to search for alternate ways of resolving this task. As expected, the above results dispute the concept of the specific difference as a significant model-independent value. This exhibits even stronger sensitivity to the models used than the HFS's themselves. On the other hand, they show that there is no fundamental problem in the interpretation of the Bohr-Weisskopf effect: by mere fitting the parameters, the effect can be equally well reproduced by either of the models within six decimals due to the appropriate choice of the model radius $R_c$. Such accuracy is quite enough for the present purposes. Naturally, the resulting $R_c$ radius turns out to be specific for the model. What various models have in common is the rms radius. Its retrieved value turns out to be similar within 1% accuracy. Such a level of description of the Bohr-Weiskopf effect shows a good prospect for the QED testing. A comparison of the obtained results to experimental data shows that the estimation of the QED effects [6] forms a good basis in this way, together with the contribution of the $e$–$e$ correlations, as calculated in Ref. [6] to the third order of the perturbation series.

Such features of the Bohr-Wesskopf effect, as established above, are in agreement with an alternative way, based on the two-parameter model, which was proposed in Ref. [8]. This way allows one to unambiguously retrieve objective characteristics of the distribution of magnetization inside the nucleus, such as the second and fourth moments. Model independence of the values thus obtained were demonstrated in Ref. [8]. Within this method, the difference obtained above in the rms values, calculated within the SC and VC models, can be attributed as a manifestation of the truncated terms, containing $R_4$ and higher moments. An analysis of the results presented

TABLE III. Comparison of various theoretical results for the HFS values $W_i$, eV, to the experiment.

| Electronic | Experiment | [8] | $\mu = 4.1106$ | [6] | $\mu = 4.092$ | |
|---|---|---|---|---|---|---|
| state $i$ | [16] | | present | | present | [16] |
| 1$s$ | 5.08503(11) | 5.0863 | 5.08584 | 5.16138 | 5.08420 | 5.089 |
| 2$s$ | 0.797645(18) | 0.7975 | 0.797645 | 0.810230 | 0.797646 | 0.7983 |

in Table III suggests that it might be impossible to describe the HFS values for the both levels simultaneously within the framework of a one-parameter model. The two-parameter method of moments [8] can be used in this case. Further research, both experimental and theoretical, is needed to better understand the above peculiarities. Specifically, measuring the $2p_{1/2}$ HFS value may be critical to this end [8]. Adding information about one more state to the database will show whether the description within the one- or two-parameter model is sufficient, or the contribution and consideration of higher multipole moments will be essential.

## ACKNOWLEDGMENTS

The authors would like to express their gratitude to L. F. Vitushkin, D. P. Grechukhin, V. M. Shabaev, and I. I. Tupitsin for fruitful discussions of the topic and helpful comments.

[1] F. F. Karpeshin, Phys. Rev. C **87**, 054319 (2013); F. F. Karpeshin and M. B. Trzhaskovskaya, Yad. Fiz. **78**, 1055 (2015); **78**, 993 (2015).
[2] V. M. Shabaev, A. N. Artemyev, V. A. Yerokhin, O. M. Zherebtsov, and G. Soff, Phys. Rev. Lett. **86**, 3959 (2001).
[3] A. Bohr and V. F. Weisskopf, Phys. Rev. **77**, 94 (1950).
[4] A. B. Migdal, *Theory of Finite Fermi Systems: and Applications to Atomic Nuclei* (Wiley Interscience, New York, 1967).
[5] J. Ullmann *et al.*, Nat. Commun. **8**, 15484 (2017).
[6] A. V. Volotka, D. A. Glazov, O. V. Andreev, V. M. Shabaev, I. I. Tupitsyn, and G. Plunien, Phys. Rev. Lett. **108**, 073001 (2012).
[7] M. Lochmann *et al.*, Phys. Rev. A **90**, 030501(R) (2014).
[8] F. F. Karpeshin and M. B. Trzhaskovskaya, Nucl. Phys. A **941**, 66 (2015).
[9] F. F. Karpeshin and M. B. Trzhaskovskaya, Yad. Fiz. **81**, 3 (2018) [Phys. At. Nucl. **81**, 1 (2018)].
[10] A. S. Reiner, Nucl. Phys. **5**, 544 (1958).
[11] F. F. Karpeshin, *Nuclear Fission in Muonic Atoms and Resonance Conversion* (Nauka, Saint Petersburg, 2006).
[12] F. F. Karpeshin and M. B. Trzhaskovskaya, Laser Phys. **17**, 508 (2007).
[13] F. F. Karpeshin, Fiz. Elem. Chastits At. Yadra **37**, 522 (2006) [Phys. Part. Nucl. **37**, 284 (2006)].
[14] L. A. Sliv, Zh. Eksp. Teor. Fiz. **21**, 770 (1951).
[15] F. F. Karpeshin, I. M. Band, M. A. Listengarten, and L. A. Sliv, Izv. Akad. Nauk SSSR. Ser. Fiz. **40**, 1164 (1976) [Bull. Acad. Sci. USSR, Phys. Ser. **40**, 58 (1976)].
[16] L. V. Skripnikov *et al.*, Phys. Rev. Lett. **120**, 093001 (2018).
[17] R. B. Firestone, *Table of Isotopes* (Wiley, New York, 1996).
[18] M. E. Rose, *Multipole Fields* (John Wiley & Sons, New-York, 1955).
[19] A. I. Akhiezer and V. B. Berestetskii, *Quantum Electrodynamics* (Wiley, New York, 1965).
[20] D. A. Varshalovich, A. N. Moskalev, and V. K. Khersonskii, *Quantum Theory Of Angular Momentum* (World Scientific, Singapore, 1988).
[21] L. D. Landau and E. M. Livshitz, *Quantum Mechanics Nonrelativistic Theory* (Pergamon, London, 1958).
[22] F. F. Karpeshin, J. Phys. G: Nucl. Part. Phys. **30**, 1 (2003).
[23] P. D. B. Collins, *An Introduction to Regge Theory and High-Energy Physics* (Cambridge University Press, Cambridge, England, 1977).
[24] I. M. Band, M. B. Trzhaskovskaya, C. W. Nestor, Jr., P. O. Tikkanen, and S. Raman, Atom. Data Nucl. Data Tables **81**, 1 (2002); **55**, 43 (1993); **35**, 1 (1986).
[25] T. Kibédi, T. W. Burrows, M. B. Trzhaskovskaya, P. M. Davidson, and C. W. Nestor, Jr., Nucl. Instrum. Meth. Phys. Res. A **589**, 202 (2008).
[26] E. Church and J. Weneser, Ann. Rev. Nucl. Sci. **10**, 193 (1960).
[27] I. M. Band, M. A. Listengarten, and A. P. Feresin, *Anomalii v Koeffitsientah Vnutrennei Konversii Gamma-Luchei* (Nauka, St. Petersburg, 1976).
[28] J. C. Hardy, N. Nica, V. E. Iacob, S. Miller, M. Maguire, and M. B. Trzhaskovskaya, Appl. Radiat. Isot. **87**, 87 (2014).
[29] S. Raman, C. W. Nestor, Jr., A. Ichihara, and M. B. Trzhaskovskaya, Phys. Rev. C **66**, 044312 (2002).
[30] M. G. H. Gustavsson and A.-M. Martensson-Pendrill, Adv. Quantum Chem. **30**, 343 (1998).
[31] F. F. Karpeshin and V. E. Starodubsky, Yad. Fiz. **35**, 1365 (1982) [Sov. J. Nucl. Phys. **35**, 795 (1982)].
[32] P. Sunnergren, H. Persson, S. Salomonson, S. M. Schneider, I. Lindgren, and G. Soff, Phys. Rev. A **58**, 1055 (1998).
[33] J. Sapirstein and K. T. Cheng, Phys. Rev. A **63**, 032506 (2001).
[34] E. Ye. Berlovich and F. F. Karpeshin, Phys. Lett. B **177**, 260 (1986).
[35] A. E. Barzakh, L. K. Batist, D. V. Fedorov, V. S. Ivanov, K. A. Mezilev, P. L. Molkanov, F. V. Moroz, S. Yu. Orlov, V. N. Panteleev, and Yu. M. Volkov, Phys. Rev. C **86**, 014311 (2012).